Available online at www.sciencedirect.com
SCIENCE DIRECT®
Solid State Nuclear Magnetic Resonance 29 (2006) 242–250
Solid State Nuclear Magnetic Resonance
www.elsevier.com/locate/ssnmr

A REDOR study of diammonium hydrogen phosphate: A model for distance measurements from adsorbed molecules to surfaces

Gil Goobes, Vinodhkumar Raghunathan, Elizabeth A. Louie[1], James M. Gibson, Gregory L. Olsen, Gary P. Drobny*

Department of Chemistry, University of Washington, Seattle WA 98115, USA

Received 13 July 2005
Available online 27 October 2005

Abstract

Magic angle spinning NMR techniques can be used to determine the molecular structure of proteins adsorbed onto polymer and mineral surfaces, but the degree to which the orientation of proteins on surfaces can be uniquely determined by NMR is less well understood. In this manuscript, REDOR data obtained from model systems are analyzed with a view to determine the orientation of rare spins coupled to a lattice populated by strongly coupled spin $\frac{1}{2}$ nuclei. When the surface is populated by closely spaced spins, the REDOR dephasing of a rare spin on the protein contact point to the surface is under certain circumstances complicated by contributions from homonuclear dipolar interactions between the spins of the lattice. To study multiple spin effects on the dephasing signal in rotational-echo-double-resonance experiments, we carried out a measurement on crystalline diammonium hydrogen phosphate as a model for a spin system with multiple dipolar interactions. Information about the ^{31}P–^{31}P interactions is gathered from the reference measurement in the experiment. To fit the experimental ^{15}N and ^{31}P dephasing data well, it was necessary to account for as many as 6 and 8 spins in simulations, respectively. Using a single spin-pair interaction with an unknown distance yielded a good fit to the ^{31}P data with a distance of 2.7 Å that is nearly an Angström shorter than the shortest distance in the crystal structure. Homonuclear couplings are shown to have a significant effect on the expected dephasing.

Keywords: Spin cluster; REDOR; SEDRA; Homonuclear couplings; Recoupling; Diammonium hydrogen phosphate; Phosphorous; Nitrogen; Surface; Protein; Biomineral

1. Introduction

Basic understanding of protein binding to solid surfaces has implications to biomaterials and biotechnological research. Hard tissue formation and implant integration are associated with an initial step of protein adsorption onto solid surfaces [1]. The assembly on the surface is often indicative of the functional role of these proteins either as bone engineers or as interfacial adaptors between the artificial device and the body. Solid-state NMR techniques can be employed to explore protein binding to biomineral surfaces. The rotational echo double resonance (REDOR) dipolar recoupling techniques [2–5] can be used to obtain distance constraints between contact points on the protein and the surface [6,7]. A single distance between a spin on the surface and a heteronuclear spin on the protein can be derived accurately using the technique. However, when several surface spins are in close proximity, the REDOR dephasing of a protein spin label becomes dependent on multiple dipolar interactions and a unique distance to the surface becomes harder to extract. Recent REDOR studies of proteins adsorbed onto hydroxyapatite have discussed the complication of data interpretation due to the presence of multiple coupled spin systems [8,9].

Past studies have investigated REDOR dephasing in multiple coupled spin systems, S–I_n, with I_n homonuclear spins, to determine whether geometrical information can be derived from the measurement [10]. Mehta and Schaefer

*Corresponding author. Fax: +1 206 685 8665.
E-mail addresses: ggoobes@u.washington.edu (G. Goobes), drobny@chem.washington.edu (G.P. Drobny).
[1]Present address: Vanderbilt University Institute of Imaging Science, Nashville, TN 37232, USA.

0926-2040/$ - see front matter © 2005 Elsevier Inc. All rights reserved.
doi:10.1016/j.ssnmr.2005.09.016

employed multiple-pulse homonuclear decoupled REDOR with *I*-spin detection to obtain individual distances when the *I*-spins are resolvable [11,12]. In most studies, detection of the *S*-spin dephasing was examined. Fyfe and Lewis have examined REDOR dephasing curves theoretically for different configurations of the S–I_2 system to explore whether REDOR dephasing can be used to deduce an unknown geometry and have concluded that different configurations give rise to similar REDOR dephasing and that incorrect distances might be derived when the spin cluster size and its geometry are completely unknown [13]. Vogt et al. have performed REDOR on 3-spin systems, i.e. S–I_2, and from REDOR data have calculated the angle between the heteronuclear dipolar coupling vectors in glycine and uracil. These authors demonstrated that angular and distance information in 3-spin systems can be obtained when the homonuclear dipolar coupling is not influencing the REDOR dephasing [14].

Goetz and Schaefer have presented a closed form numerical algorithms to calculate REDOR dephasing for many-spin systems undergoing rapid motional exchange that make all dephasing spins magnetically equivalent. In this limit homonuclear couplings do not affect the REDOR dephasing [15]. Bertmer and Eckert have predominantly used numerical simulations to probe the information content available in multi-spin REDOR experiments and have extracted an effective dipolar coupling constant from the early part of the dephasing curve using a second moment analysis [16]. Chan and Eckert have shown that homonuclear couplings alter the dephasing in REDOR even when they are significantly smaller than the spinning frequency. They developed a modified version of REDOR called the C-REDOR, to remove the effect of homonuclear couplings [17].

As a model for a ^{15}N nucleus in a protein sidechain in close proximity to a calcium phosphate surface, we carried out REDOR measurements on undiluted polycrystalline diammonium hydrogen phosphate (DHP) to investigate the size of the spin system involved in REDOR dephasing in tightly coupled spin systems. We show that the dephasing observed in the ^{31}P REDOR reference experiment can be accurately associated with ^{31}P–^{31}P dipolar couplings based on nearest-neighbor distances in the crystal and that for DHP at least 5 ^{31}P–^{15}N dipolar couplings to the nearest nitrogen atoms as well as nearest ^{31}P atoms must be included in calculations to simulate accurately the acquired REDOR dephasing. Similarly, the ^{15}N REDOR dephasing is well simulated taking into account two crystallographically unique nitrogen atoms with 4 and 5 nearest ^{31}P spins.

To simulate dephasing scenarios of a ^{15}N spin to the surface of DHP crystallite, we have taken a cross-section of the crystal along the [4,0,0] direction and defined a 4-spin cluster of ^{31}P nuclei as the interacting surface spin bath. Calculations of XY-REDOR dephasing at different distances to the ^{31}P cluster show that it will be possible to measure the distance of the nitrogen to the surface with somewhat lower accuracy than in an isolated spin pair case. Homonuclear couplings amongst the spins in the surface bath have a non-negligible contribution that causes leveling off of the dephasing curve and may complicate extraction of accurate distance unless accounted for in simulations. We suggest in this manuscript that REDOR experiments performed on rare spins in protein side chains coupled to a bath of strongly coupled spin systems in biomaterial surfaces could be successfully interpreted provided that the bath is simulated by a large enough spin system and that the interactions between the spins in the bath are accounted for in the simulations.

2. Analytical theory

We assume a single rare spin $\frac{1}{2}$ nucleus S (e.g. ^{15}N, ^{13}C, etc.) dipolar coupled to a bath of spin $\frac{1}{2}$ nuclei I_1, I_2, $I_{3...}I_N$ (e.g. ^{31}P, ^{19}F, etc.), as shown in Fig. 1. We assume at first that all *I*-spins are dipolar coupled to the *S* spin. We also assume that the *I*-spins are dipolar coupled to one another.

The problem before us is to determine under what circumstances homonuclear dipolar interactions within the *I*-spin bath influence the REDOR dephasing of the *S*-spin. We assume in this treatment that the REDOR pulse sequence with XY-4 cycling [18] of the phases is applied to both S and I channels, but the arguments can be generalized to the commonly used XY-8 phase cycling version (see Fig. 2). In XY-4 the phases of the π-pulses in both the observed and dephasing channels alternate as $(xyxy)_N$, while the phases in XY-8 are symmetrized $(xyxyyxyx)_N$, where N designates the number of REDOR cycles.

The spin interaction Hamiltonian for the system, schematized in Fig. 1, is

$$\begin{aligned} H_{\mathrm{int}}(t) &= H_S(t) + H_I(t) + H_{IS}(t) + H_{II}(t) \\ &= \omega_{\mathrm{S}}(t)S_Z + \sum_{i=1}^{N} \omega_{\mathrm{I}^i}(t)I_Z^i + S_Z \sum_{i=1}^{N} \omega_{SI^i}(t)I_Z^i \\ &\quad + \sum_{i\neq j} \omega_{ij}(t)(I_Z^i I_Z^j - \tfrac{1}{4}(I_+^i I_-^j + I_-^i I_+^j)), \end{aligned} \tag{1}$$

where $H_S(t)$ is the chemical shielding Hamiltonian of the *S*-spin, $H_I(t)$ is the chemical shielding Hamiltonian of the *I*-spins, $H_{IS}(t)$ accounts for the heteronuclear dipolar couplings between the *S*-spin and the *I*-spin bath, and

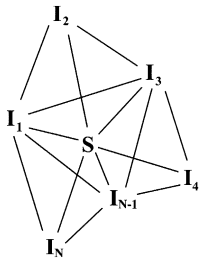

Fig. 1. A schematic representation of a rare spin *S*, coupled to a cluster of closely interacting *I* spins.

$H_{II}(t)$ accounts for the homonuclear dipolar couplings between members of the I-spin bath. The time dependence attached to these Hamiltonians is due to rotation of these anisotropic interactions around an axis inclined at the "magic angle" with respect to the static field.

In Fig. 3 we show the spin angular momentum operators viewed from a "toggling" or interaction frame defined by the radio frequency (r.f.) Hamiltonian for XY-4 REDOR. The REDOR π-pulses in this derivation are taken to be infinitely strong. The operators for the S-spin toggle on the full cycle and for the I-spins on the half-cycle. XY-8 essentially continues this toggling through 8 rotor cycles.

The effective REDOR evolution runs over the 4 rotor cycles and terminates immediately after the fourth S pulse when the r.f. propagator concludes its period, i.e.

$$U_{\text{XY-4}}(t) = U_{\text{XY-4}}(t + 4\tau_R), \tag{2}$$

where the r.f. propagator is defined as

$$U_{\text{XY-4}} = T\exp\left[-\mathrm{i}\int_0^t H_{\text{r.f.}}^{\text{XY-4}}(t')\,\mathrm{d}t'\right] \tag{3}$$

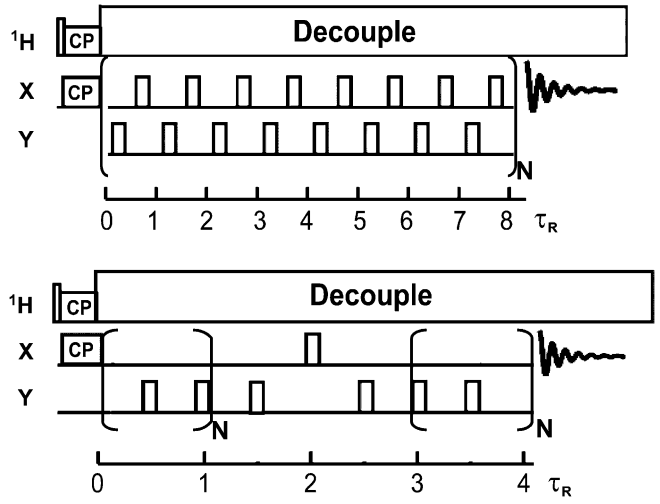

Fig. 2. Different REDOR pulse sequences: (top) with alternating π-pulses (bottom) with a single π-pulse on the observe channel and the rest on the dephasing channel. The experiment is carried out by incrementing the pulses N times and recording the signal obtained as a function of N. For XY-4 phase cycling (top), the basic cycle is of 4 pulses rather than 8.

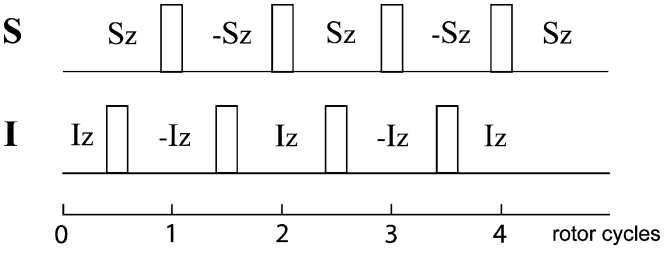

Fig. 3. Toggling frame representation of the spin operators in the XY-REDOR pulse sequence at different points along the time propagation of the experiment.

and where τ_R is the rotor period and T is the Dyson time ordering operator. After 4 rotor cycles the spin interaction propagator is

$$U_{\text{int}}(t_C = 4\tau_R) = \prod_{k=1}^{8}\exp\left[-\mathrm{i}\int \tilde{H}_{\text{int}}^{k}(t')\,\mathrm{d}t'\right], \tag{4}$$

where each integration is over the duration of the kth half-rotor cycle, and the interaction frame Hamiltonian toggles discretely with the r.f. through the 8 half-cycles as

$$\tilde{H}_{\text{int}}^{k}(t) = U_{\text{XY-4}}^{-1}(k)H_{\text{int}}(t)U_{\text{XY-4}}(k), \tag{5}$$

where $U_{\text{XY}-4}(k)$ denotes the r.f. propagator for k half-rotor cycles.

Using the Hamiltonian in Eq. (1), average Hamiltonian theory (AHT) [19–21] can be used to calculate the contribution of the homonuclear coupling between the bath spins to the dephasing of the S spin being irradiated by XY-4 pulses. According to AHT, the r.f. cycle propagator can be written in the form

$$\begin{aligned} U_{\text{int}}(t_C) &= \prod_{k=1}^{8}\exp\left[-\mathrm{i}\int \tilde{H}_{\text{int}}^{k}(t')\,\mathrm{d}t'\right] \\ &= \exp\left[-\mathrm{i}t_C(\bar{H}^{(0)} + \bar{H}^{(1)} + \bar{H}^{(2)} + \ldots)\right], \end{aligned}$$

where

$$\begin{aligned} \bar{H}^{(0)} &= \frac{1}{t_C}\int_0^{t_C}\tilde{H}_{\text{int}}(t)\,\mathrm{d}t, \\ \bar{H}^{(1)} &= \frac{-i}{2t_C}\int_0^{t_C}\mathrm{d}t_2\int_0^{t_2}\mathrm{d}t_1[\tilde{H}_{\text{int}}(t_2), \tilde{H}_{\text{int}}(t_1)], \\ \bar{H}^{(2)} &= \frac{-1}{6t_C}\int_0^{t_C}\mathrm{d}t_3\int_0^{t_3}\mathrm{d}t_2\int_0^{t_2}\mathrm{d}t_1 \\ &\quad\times\{[\tilde{H}_{\text{int}}(t_3),[\tilde{H}_{\text{int}}(t_2), \tilde{H}_{\text{int}}(t_1)]] \\ &\quad+[[\tilde{H}_{\text{int}}(t_3), \tilde{H}_{\text{int}}(t_2)], \tilde{H}_{\text{int}}(t_1)]\}. \end{aligned} \tag{6}$$

Here we calculate the zeroth and first-order terms. The interaction frame Hamiltonian for the first half-rotor cycle is

$$\begin{aligned} \tilde{H}_{\text{int}}^{1} &= \omega_S(t)S_Z + \sum_{i=1}^{N}\omega_{I^i}(t)I_Z^i + S_Z\sum_{i=1}^{N}\omega_{SI^i}(t)I_Z^i \\ &\quad+\sum_{i\neq j}\omega_{ij}(t)(I_Z^iI_Z^j - \tfrac{1}{4}(I_+^iI_-^j + I_-^iI_+^j)). \end{aligned} \tag{7}$$

To calculate $\bar{H}^{(0)}$, we expand each time-dependent spin interaction as a Fourier series

$$\omega_\lambda(t) = \sum_{m=-2}^{+2}\omega_\lambda^{(m)}\mathrm{e}^{\mathrm{i}m\omega_R t}, \tag{8}$$

where λ indicates the spin interaction. Expressions for the complex coefficients $\omega_\lambda^{(m)} = a_\lambda^{(m)} + \mathrm{i}b_\lambda^{(m)}$ can be found in Ref. [22]. Inspection of Fig. 3 indicates that $\bar{H}^1 = \bar{H}^5$, $\bar{H}^2 = \bar{H}^6$, $\bar{H}^3 = \bar{H}^7$, and $\bar{H}^4 = \bar{H}^8$. With these facts and

using standard methods the average Hamiltonian is

$$\bar{H}^{(0)} = -\frac{2}{8\pi} \times 4 \times 4 \sum_{k=1}^{N} b_{SI^k}^{(1)} I_Z^k S_Z = -\frac{4}{\pi} \sum_{k=1}^{N} b_{SI^k}^{(1)} I_Z^k S_Z. \quad (9)$$

Eq. (9) just states that, as expected, to lowest order the response of the spin system to XY-4 irradiation is to dephase under the heteronuclear dipolar interaction.

XY-4 and XY-8 are designed to compensate for pulse imperfections and frequency offset. However, these sequences are not symmetric in time in the sense that $\tilde{H}_{\mathrm{int}}(t) \neq \tilde{H}_{\mathrm{int}}(t_C - t)$. Lack of cycle symmetry means that for XY-4 and XY-8 the first-order term in the Magnus expansion ($\bar{H}^{(1)}$ in Eq. (6)) is non-zero. Calculating this term, it is straightforward to determine a coupling between the heteronuclear dipolar interaction and the homonuclear couplings within the bath. In general, the commutator between the heteronuclear dipolar Hamiltonian and the homonuclear dipolar "bath Hamiltonian" is given by

$$\left[S_Z \sum_{j=1}^{N} \omega_{SI^j}(t) I_Z^j, \sum_{j \neq k} \omega_{jk}(t) (I_Z^j I_Z^k - \tfrac{1}{4}(I_+^j I_-^k + I_-^j I_+^k)) \right] = -\frac{S_Z}{4} \sum_{j \neq k} (\omega_{SI^j}(t) - \omega_{SI^k}(t)) \omega_{jk}(t) (I_+^j I_-^k - I_-^j I_+^k). \quad (10)$$

Eq. (10) states that if an S spin is coupled inequivalently to a pair of bath-spins the homonuclear coupling between the bath-spins will contribute to first order. The homonuclear coupling may also enter the REDOR response to second order given inequivalent heteronuclear couplings. Eq. (10) also implies that if an S spin is coupled to a bath of strongly coupled spins but if, due to a symmetrical molecular motion the heteronuclear couplings are equal, homonuclear couplings between bath spins do not contribute to any order when the bath spins are magnetically equivalent. This is the circumstance encountered by Goetz and Schaefer [15], who studied the REDOR response of a ^{13}C spin coupled to 3 ^{19}F spins in a CF_3 group. No symmetrical motion exists in DHP that would equalize the ^{15}N–^{31}P couplings, so homonuclear couplings between dephasing spins should affect the REDOR dephasing according to Eq. (10).

3. Materials and methods

The compound [$^{15}N_2$] diammonium hydrogen phosphate $(NH_4)_2HPO_4$ was purchased from Sigma-Aldrich. Solid-state NMR measurements were conducted on it without dilution or recrystallization. ^{31}P Simple Experiments for the Dephasing of Rotational-echo Amplitude (SEDRA) were carried out on a home-built 4.7 T spectrometer equipped with a 5 mm triple-tuned ^{1}H–^{19}F–^{31}P transmission-line probe. Phosphorous spins were cross polarized using a contact time of 2 ms. Phosphorous 180° pulses at a field of 22 kHz were employed using a cycling of the pulse phase according to the XY8 scheme [18]. Continuous wave decoupling at a field of 73 kHz was used during the whole experiment. Experiments were carried out at a spinning rate of 2557 Hz. ^{31}P–^{15}N and ^{15}N–^{31}P REDOR measurements were carried out on a home-built wide-bore 11.7 T spectrometer using a Varian 4 mm ^{1}H-^{31}P–^{15}N triple-tuned probe. Phosphorous cross polarization was achieved using a ramped field between 52 and 26 kHz on the protons and a field of 34 kHz on the phosphorous for 2 ms. Nitrogen cross polarization was achieved using a ramped field between 46 and 23 kHz on the protons and a field of 30 kHz on the nitrogen for 3 ms. Phosphorous and nitrogen 180° pulses at fields of 62 and 45 kHz, respectively, were used through all REDOR experiments. Continuous wave decoupling at a field of 85 kHz was used during the entire experiment. Experiments were carried out at a spinning rate of 4000 Hz.

3.1. Spin dynamics simulations

Calculations were carried out with SPINEVOLUTION [23] and SIMPSON [24] spin dynamics programs. Convergence of results from the two programs was verified for simulations of up to 5-spin systems. For larger spin clusters (up to 9 spins) the SPINEVOLUTION program was used. The minimal set of $\{\alpha, \beta\}$ Euler angle pairs used in powder averaging was 54 as specified by the Zaremba–Conroy–Wolfsberg scheme [25,26] and 5 γ-angles. Larger crystallite sets showed insignificant changes in calculated dephasing. The ^{31}P chemical shift anisotropy and asymmetry parameters were derived from the cross polarization magic angle spinning (CPMAS) spectra and confirmed against known values [27]. Directions of the ^{31}P CSA tensor principal components in the molecular frame [28–30] were used to derive relative P–P CSA orientations (Euler angles) based on phosphate group orientation in the crystal structure [31]. The CSA of the ^{15}N nucleus in the molecule was found to be small and was therefore neglected. All dipolar interaction parameters were computed from distances and orientations of P–P and P–N vectors in the crystal and referenced to the CSA PAS frame of the observed P atom in calculations.

4. Results

4.1. Crystal structure

DHP crystallizes in the $P2_1/c$ space group with unit cell dimensions of $a = 11.04$ Å, $b = 6.70$ Å and $c = 8.03$ Å [31]. Each unit cell contains 4 molecules that are symmetry related and are closely packed. Subsets of 3×3 unit cells from the crystal structure depicting the surroundings of the phosphorus and the nitrogen atoms are shown in Fig. 4. P–N distances that are within 3.99 Å and P–P distances that are shorter than 4.44 Å are denoted in the top picture. Similarly, N–P distances within 4.11 Å are denoted in the bottom picture. The distances given in the figure and the corresponding dipolar interaction constants are summarized in Table 1. The two nitrogen atoms in the ammonium

groups, annotated by N1 and N2 in the figure, are crystallographically inequivalent and are slightly chemically shifted from each other. The phosphate groups are identical and appear as a single line in the ^{31}P CPMAS spectrum.

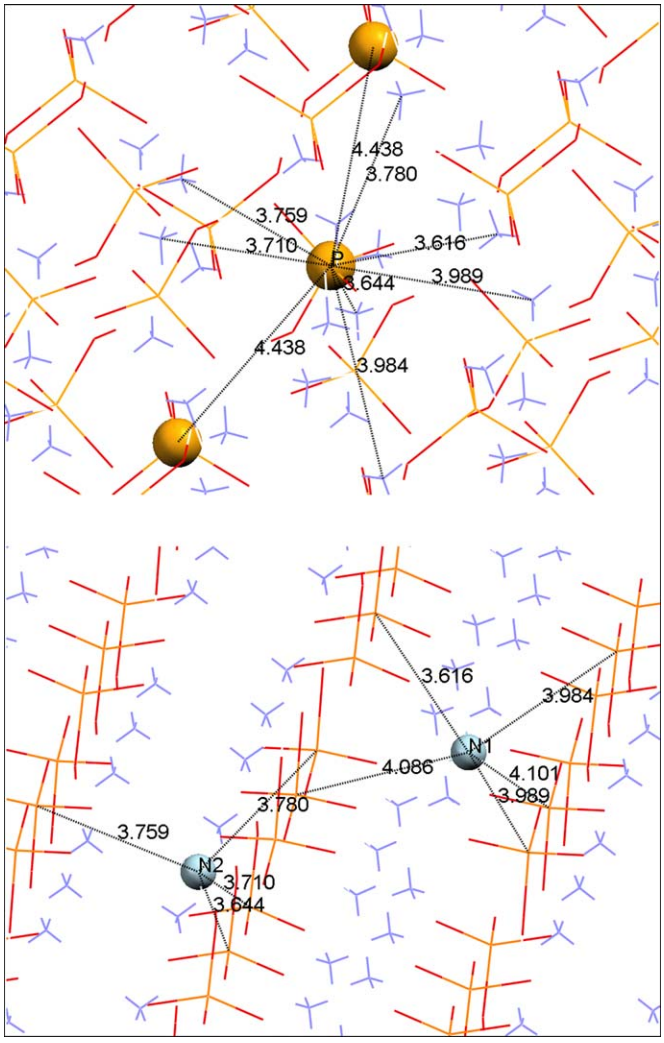

Fig. 4. Crystal Structure of DHP depicting the closest P (large spheres) and N neighbors to a central P atom (top) and the closet P neighbors to the N1 and N2 atoms (small spheres) (bottom) in a 3×3 unit cell subset. All distances shown in the figure are in units of Å.

4.2. Experimental results

^{15}N–^{31}P and ^{31}P–^{15}N REDOR experiments were carried out on DHP. The REDOR pulse technique can be carried out in different ways. Experiments having 1 refocusing π-pulse in the middle of the sequence in the observe channel and all the rest of the π-pulses on the dephase channel (Fig. 2 bottom) are plainly termed here REDOR experiments. Experiments having the π-pulses alternating between the observe and dephase channels (Fig. 2 top) are termed here XYn-REDOR with n equal to either 4 or 8 depending upon the scheme used to cycle the phases of the pulses. The REDOR results in this work are shown as a ratio of the dephasing S signal normalized to the reference S_o signal. Experimental errors, derived from signal to noise ratios in the acquired data, are used to calculate error bars. Whenever measurements were repeated, a combination of experimental error and standard deviation due to data distribution is used to deduce the error bars.

4.3. ^{31}P SEDRA

The normalized S_o signal decay in the ^{31}P XY8-REDOR experiment performed at a field of 4.7 T (squares) and at a field of 11.7 T (circles) is shown in Fig. 5. A relaxation model could not fit the decay curves. The observed spin is dephasing due to coupling of the ^{31}P spin to adjacent ^{31}P spins in the crystal, and the experiment is therefore comparable to the SEDRA experiment [32]. We utilized this fact to independently verify the ^{31}P–^{31}P couplings from distances in the crystal. Simulations of ^{31}P signal dephasing using the two largest P–P couplings given in Table 1, due to SEDRA-type of homonuclear recoupling, gave excellent fit to both datasets. Transverse relaxation rates of 90 and 20 Hz for the 11.7 and 4.7 T data, respectively, were incorporated in these calculations to account for additional slower decay of the magnetization [33]. The difference in ^{31}P SEDRA dephasing at 11.7 and 4.7 T arises solely from difference in relaxation rates. Calculations without relaxation damping at the two fields are nearly identical despite the large differences in the ^{31}P CSA size. To determine how effective the measurement for deducing the dipolar coupling and CSA parameters is, simulations at variable

Table 1
The shortest distances and the corresponding dipolar couplings between pairs of atoms in the crystalline DHP

P–P distance/coupling strength	P–N1 distance/coupling strength	P–N2 distance/coupling strength	N–N distance/coupling strength
4.44 Å/−225 Hz	**3.62 Å/104 Hz**	**3.64 Å/102 Hz**	3.54 Å/−28 Hz
4.44 Å/−225 Hz	**3.98 Å/78 Hz**	**3.71 Å/97 Hz**	3.63 Å/−26 Hz
5.40 Å/−125 Hz	**3.99 Å/78 Hz**	**3.76 Å/93 Hz**	
6.10 Å/−87 Hz	**4.09 Å/72 Hz**	**3.78 Å/91 Hz**	
6.27 Å/−80 Hz	**4.10 Å/72 Hz**		

Bold values represent values used in ^{15}N–^{31}P simulations and underlined ones represent values used in the ^{31}P–^{15}N simulations. The N–N values were neglected due to their relatively small size. Other adjacent P atoms that interact with the central P spin in the system constructed have smaller coupling values and were therefore omitted to limit the spin cluster size.

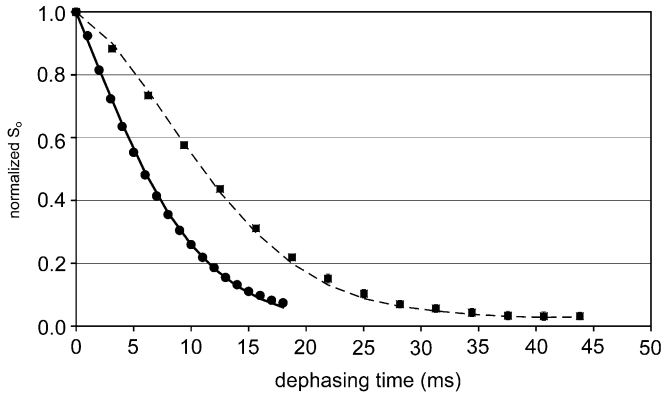

Fig. 5. ^{31}P XY-REDOR S_o (SEDRA) dephasing curves at two different fields. The circles indicate the data acquired with a homemade spectrometer operating at 11.4 T and the squares indicate data acquired at 4.7 T. The dashed and solid lines indicate the respective SEDRA simulations for the lower and higher field measurements.

values must be carried out. It is beyond the scope of this study; therefore here we restricted our investigation to reproduction of experimental data through simulations relying on the known interaction parameters.

4.4. ^{31}P–^{15}N REDOR

The good fit achieved in the SEDRA measurements indicated that coupling to the two nearest spins governs the ^{31}P dynamics and is sufficient to be considered in ^{31}P–^{15}N REDOR simulations. ^{31}P–^{15}N XY4-REDOR (empty diamonds) and XY8-REDOR (filled circles) results gave rise to similar signal dephasing as shown in Fig. 6 (top) and are fitted well by simulations taking into account 3 ^{31}P spins and 5 ^{15}N spins with dipolar coupling constants as given in Table 1. Similarly, ^{31}P–^{15}N REDOR data (filled circles), plotted in the bottom of Fig. 6, were fitted well with the same 8-spin system subject to the REDOR pulse sequence.

The dependence of REDOR simulations on the size of the spin system is demonstrated in Fig. 7. The same ^{31}P XY8-REDOR data shown before in Fig. 6 are plotted with 4 calculated curves. The dotted line corresponds to calculation taking into account the 3 ^{31}P spins and the closest ^{15}N spin (P3N1). The dashed line corresponds to calculation taking into account the 3 ^{31}P spins and the 3 closest ^{15}N spins (P3N3). The thick solid line corresponds to calculation taking into account the 3 ^{31}P spins and the 5 closest ^{15}N spins (P3N5). Other simulations carried out for P3N4, P3N6 and P3N7 (data not shown) show that for spin systems smaller than P3N5 deviations of the calculation from experimental data are too large to predict the dephasing reasonably; however, for systems larger than P3N5 the net effect of additional heteronuclear spins does not alter the curve substantially. The thin solid line corresponds to calculation based on unknown size and configuration of the ^{31}P spin cluster where a single ^{31}P–^{15}N pair is assumed. In this case the calculation that best fits the experimental data gives rise to a heteronuclear dipolar

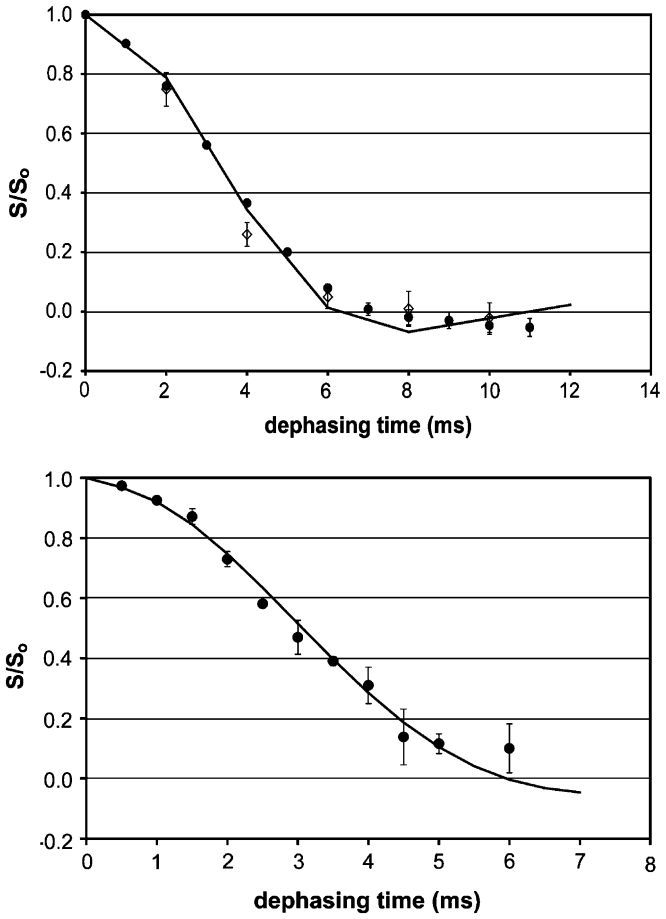

Fig. 6. (Top) ^{31}P–^{15}N REDOR dephasing data of DHP acquired using XY8 (filled circles) and XY4 REDOR (empty diamonds) pulse sequences. The solid line is the XY8 REDOR simulation taking into account all the nearest neighbors (a P3N5-spin system) of a central ^{31}P spin. (Bottom) ^{31}P–^{15}N REDOR dephasing data (filled circles) acquired using the REDOR pulse sequence. The solid line is the REDOR simulation using the same P3N5 spin system as above.

interaction of 230 Hz and to a distance of 2.78 Å. This distance is 0.9 Å shorter than the shortest PN distance in the crystal structure.

4.5. ^{15}N–^{31}P REDOR

^{15}N-detected experiments were carried out on DHP as well. The XY8-REDOR S_o experiment (data not shown) exhibits no dephasing due to homonuclear dipolar interaction. The ^{15}N–^{15}N couplings are too weak to show any appreciable dephasing within the transverse relaxation time. The XY-REDOR and REDOR results are shown in Fig. 8 top and bottom graphs, respectively. As seen in the ^{31}P case, the XY4- (filled circles) and the XY8-REDOR data (empty circles) decay at identical rates. All simulations shown as lines in Fig. 8 were done using 2 separate calculations. Dephasing of N1 by its 5 closest ^{31}P neighbors and dephasing of N2 spin by its 4 nearest ^{31}P spins were combined to the weighed average dephasing experienced by the N spin. Both XY8-REDOR (top) and REDOR

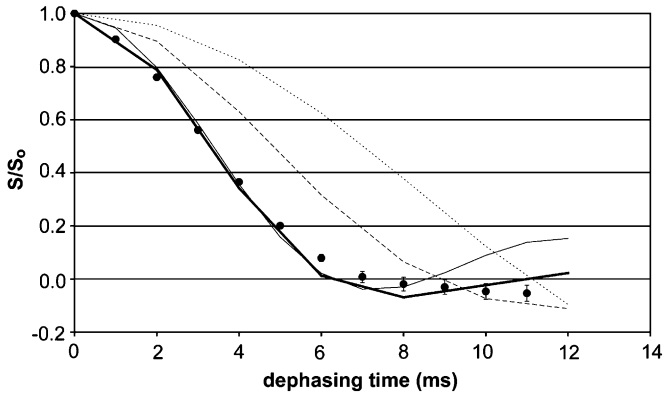

Fig. 7. Fitting of the ^{31}P–^{15}N XY8 REDOR dephasing data (filled circles) as a function of the spin cluster size. The dotted line represents a P3N1 simulation, the dashed line is a P3N3 simulation and the thick solid line is a P3N5 simulation that includes seven nearest neighbors. The REDOR data may also mistakenly be simulated using a single PN pair dephasing with an effective dipolar coupling of 230 Hz (thin solid line) had the spin cluster size been unknown.

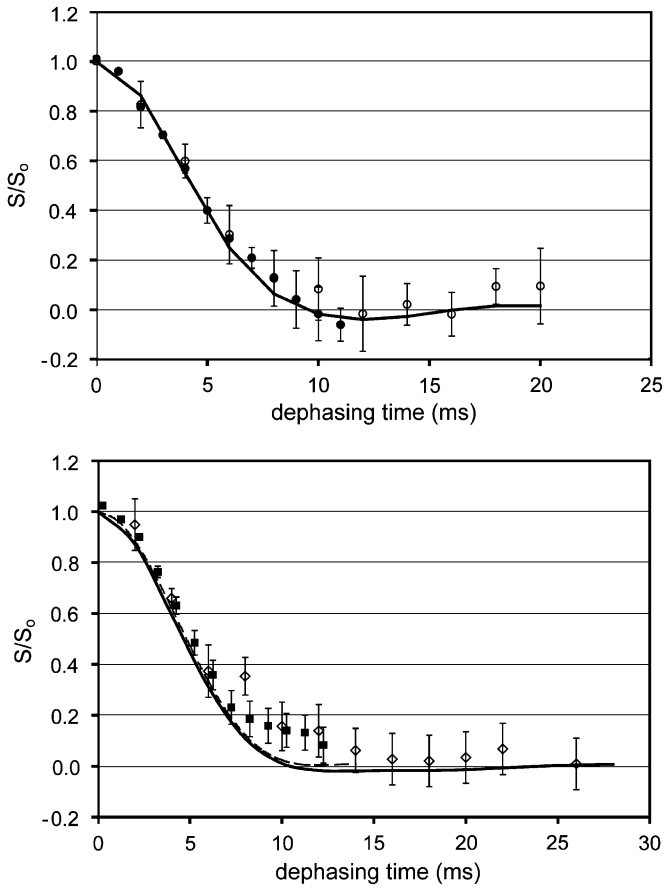

Fig. 8. ^{15}N–^{31}P REDOR dephasing of diammonium hydrogen phosphate. (Top) XY4 (filled circles) and XY8 (empty circles) REDOR at 4 kHz spinning speed (bottom) REDOR at both 4 kHz (empty diamonds) and 8 kHz (filled squares) spinning speeds. The dashed and solid lines are the weighted average of the ^{15}N REDOR dephasing simulations from the N1 and from the N2 spins at 4 and 8 kHz, respectively.

(bottom) show very good fit to experimental data. REDOR data (filled squares) and simulations (dashed line) were carried out at a spinning rate of 8 kHz as well. The data and simulations do not show any substantial difference in dephasing relative to the data at a spinning rate of 4 kHz. The simulations did not show any appreciable difference in REDOR dephasing for the two crystallographically different ^{15}N sites (data not shown). The observed ^{31}P REDOR decay is faster than the ^{15}N one because overall it has more heteroatom neighbors and is hence subjected to a stronger dephasing heteronuclear dipolar field.

4.6. Simulations of ^{15}N REDOR dephasing from a planar arrangement of ^{31}P spins

Simulations of ^{31}P–^{15}N and ^{15}N–^{31}P REDOR data taken from DHP together with analytical theory show that homonuclear couplings between spins of the dephasing bath will affect the REDOR dephasing. The size of the spin system used to simulate the dephasing bath was also shown to be germane. Because these conditions prevail for REDOR data acquired for a rare spin on the side chain of an adsorbed protein and the ^{31}P spins at the surface of a biological apatite, we studied the degree to which the orientation of the rare spin to the surface dephasing bath compromises the degree to which heteronuclear couplings can be quantified from REDOR data and used to determine internuclear distances. Figs. 9 and 10 show simulations of ^{15}N XY8-REDOR signal coupled to a planar array of 4 ^{31}P spins. The ^{15}N is taken to be a spin label on a molecule that interacts with a surface. The 4 ^{31}P spins are in planar arrangement as derived from a cross section of the crystal structure of DHP along the [4,0,0] plane and as illustrated in Fig. 9 (inset). ^{15}N distances of

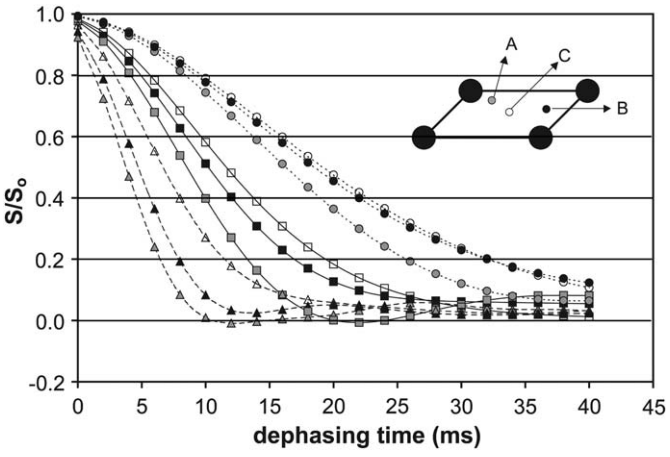

Fig. 9. ^{15}N XY8 REDOR dephasing curves of a single N atom approaching the surface created by slicing the diammonium hydrogen phosphate crystal along the [4,0,0] plane at different vertical distances. The cross-section consists of 4 phosphorous atoms in a parallelogram lattice of lengths 4.44 and 6.77 Å. Triangles, squares and circles denote a vertical distance of 3, 4 and 5 Å, respectively. The lateral positions, shown in the inset, correspond to simulations with similar symbol filling.

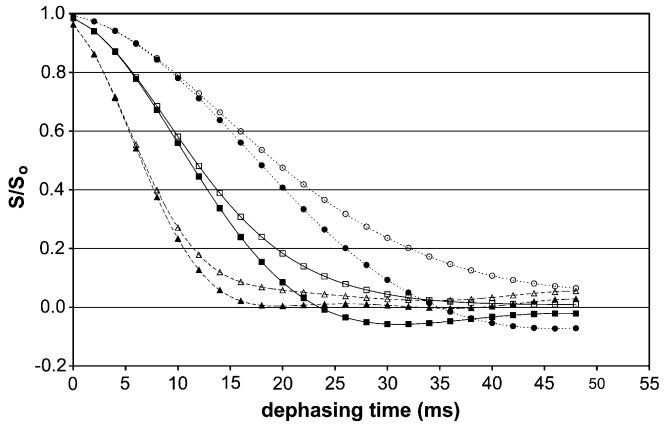

Fig. 10. Simulations of the ^{15}N XY8 REDOR dephasing in a spin cluster as shown in Fig. 9 turning the phosphorous homonuclear couplings on (empty symbols) and off (filled symbols). The triangles represent a vertical distance of 3 Å, the squares represent a vertical distance of 4 Å and the circles, a distance of 5 Å.

3 Å (dashed lines), 4 Å (solid lines) and 5 Å (dotted lines) from the plane defined by the ^{31}P cluster are considered in Fig. 9. Different lateral positions of the ^{15}N normal to the ^{31}P plane are denoted by gray-filled (A), black-filled (B) and empty (C) symbols for each distance. The simulations show that at close proximities and for that specific configuration of the ^{31}P spin cluster the distance and the relative lateral position of the ^{15}N spin can be determined to better than 0.5 Å at mixing times less than 15 ms, but in general the accuracy is limited by variability in the lateral position of the ^{15}N spin relative to the surface lattice. As the distance from the cluster increases, the divergence of dephasing at different lateral positions decreases but the accuracy of distance determination is expected to improve. The presence of any other interaction on the rare ^{15}N spin such as large CSA, homonuclear interaction to another ^{15}N spin or a distribution of distances to the spin bath is likely to complicate analysis and may require additional measurements to quantitate these interactions independently.

Fig. 10 demonstrates the effect of homonuclear interactions in the ^{31}P cluster on ^{15}N REDOR dephasing. ^{15}N distances of 3 Å (dashed lines), 4 Å (solid lines) and 5 Å (dotted lines) to ^{31}P cluster parallelogram center are demonstrated in Fig. 10. The curves with filled symbols depict calculations devoid of the homonuclear couplings whereas the empty symbols ones depict calculations that include the couplings. The extent of effect of the homonuclear interactions in the ^{31}P spin cluster on the dephasing of the ^{15}N spin is apparent in all distances but gets more pronounced with increased ^{15}N distance. The REDOR dephasing is leveling off at higher values with increased distance when the homonuclear couplings are considered.

5. Conclusions

The results obtained from REDOR measurements in polycrystalline diammonium hydrogen phosphate demonstrate that in coupled spin systems where sufficient knowledge about interaction parameters is known, it is possible to accurately simulate the expected dephasing. The size of the spin system considered in simulations is important and is generally dependent on the relative sizes of the couplings experienced by the observed spin. For the ^{31}P REDOR data, it was shown that as many as 8 spins need to be included to obtain a good fit to data and increasing the system size beyond this point has no substantial effect on the calculation. The homonuclear couplings were shown to affect the ^{31}P dephasing observed and simulations of an ^{15}N spin interacting with a plane of 4 coupled ^{31}P spins predict a significant contribution that appears as a leveling off of the dephasing signal. Finally, it was shown that potentially one could measure the proximity of a spin from a surface with a tightly coupled spin cluster. The accuracy of distance measurement will be reduced when the heteronuclear couplings are of similar magnitude to the homonuclear couplings in the spin bath, but will increase as the rare spin is further removed from the surface. In that case, though, the lateral dependence is expected to diminish.

While our data indicate that REDOR data can be simulated and heteronuclear couplings determined with better than 0.5 Å accuracy when the surface spin-bath is accurately represented and not truncated in simulations, a combination of NMR techniques will likely be necessary to determine the geometry of the surface spin-bath. Homonuclear recoupling NMR techniques and/or spin cluster analysis by multiple quantum NMR may be useful approaches in acquiring this kind of information.

Acknowledgments

This work was supported by the National Science Foundation (EEC-9529161 and DMR-0110505) and the National Dental Institute (DE-12554). J.M.G. is supported by a training grant from the National Institute of Dental and Craniofacial Research (DE-07023).

References

[1] J.J. Gray, Curr. Opin. Struct. Biol. 14 (2004) 110–115.
[2] T. Gullion, J. Schaefer J. Magn. Reson. 81 (1989) 196–200.
[3] T. Gullion, Concepts Magn. Reson. 10 (1998) 277–289.
[4] T. Gullion, J. Schaefer, Adv. Magn. Reson. 13 (1989) 57–83.
[5] T. Gullion, Magn. Res. Rev. 17 (1997) 83.
[6] G.P. Drobny, J.R. Long, T. Karlsson, W.J. Shaw, J. Popham, N. Oyler, P. Bower, J. Stringer, D. Gregory, M. Mehta, P.S. Stayton, Annu. Rev. Phys. Chem. 54 (2003) 531–571.
[7] P.S. Stayton, G.P. Drobny, W.J. Shaw, J.R. Long, M. Gilbert, Crit. Rev. Oral Biol. Med. 14 (2003) 370–376.
[8] W.J. Shaw, A.A. Campbell, M.L. Paine, M.L. Snead, J. Biol. Chem. 279 (2004) 40263–40266.
[9] J.M. Gibson, V. Raghunathan, J.M. Popham, P.S. Stayton, G.P. Drobny, J. Am. Chem. Soc. 127 (2005) 9350–9351.
[10] A. Naito, K. Nishimura, S. Tuzi, H. Saito, Chem. Phys. Lett. 229 (1994) 506;
M. Hologneа, P. Bertania, T. Azais, C. Bonhomme, J. Hirschinger, Solid State Nucl. Magn. Reson. 28 (2005) 50–56.
[11] J. Schaefer, J. Magn. Reson. 137 (1999) 272–275.

[12] A.K. Mehta, J. Schaefer, J. Magn. Reson. 163 (2003) 188–191.
[13] C.A. Fyfe, A.R. Lewis, J. Phys. Chem. B 104 (2000) 48–55.
[14] F.G. Vogt, J.M. Gibson, S.M. Mattingly, K.T. Mueller, J. Phys. Chem. B 107 (2003) 1272–1283.
[15] J.M. Goetz, J.J. Schaefer, J. Magn. Reson. 127 (1997) 147–154.
[16] M. Bertmer, H. Eckert, Solid State Nucl. Magn. Reson. 15 (1999) 139–152.
[17] J.C.C. Chan, H. Eckert, J. Chem. Phys. 115 (2001) 6095–6105.
[18] T. Gullion, D.B. Baker, M.S. Conradi, J. Magn. Reson. 89 (1990) 479–484.
[19] U. Haeberlen, High Resolution NMR in Solids: Selective Averaging, in: Advances in Magnetic Resonance, Suppl. 1, Academic Press, New York, 1976.
[20] M. Mehring, Principles of High Resolution NMR in Solids, second ed., Springer, New York, 1983.
[21] M.H. Levitt, D.P. Raleigh, F. Creuzet, R.G. Griffin, J. Chem. Phys. 92 (1990) 6347–6364.
[22] A.E. Bennett, R.G. Griffin, S. Vega, in: NMR Basic Princ. Progr. (Solid-State NMR IV: Methods Appl. Solid-State NMR) 33 (1994) 1–77.
[23] M. Veshtort, R.G. Griffin, J. Chemphyschem. 6 (2004) 834–850.
[24] M. Bak, J.T. Rasmussen, N.C. Nielsen, J. Magn. Reson. 147 (2000) 296–330.
[25] H. Conroy, J. Chem. Phys. 47 (1967) 5307–5318.
[26] V.B. Cheng, H.H. Suzukawa, M. Wolfsberg, J. Chem. Phys. 59 (1987) 3992–3999.
[27] T.M. Duncan, Chemical Shift Tensors, Farragut Press, Madison, WI, 1997.
[28] J. Herzfeld, R.G. Griffin, R.A. Haeberkorn, Biochemistry 17 (1978) 2711–2718.
[29] S. Un, M.P. Klein, J. Am. Chem. Soc. 111 (1989) 5119–5124.
[30] S.J. Kohler, J.D. Ellett, M.P. Klein, J. Chem. Phys. 64 (1976) 4451–4458.
[31] A.A. Khan, J.P. Roux, W.J. James, Acta Crystallogr. B 28 (1978) 2065–2069.
[32] T. Gullion, S. Vega, Chem. Phys. Lett. 194 (1992) 423–428.
[33] G. Goobes, S. Vega, J. Magn. Reson 154 (2002) 236–251.